Motion of polar cap arcs

K. Hosokawa,[1,2] J. I. Moen,[2] K. Shiokawa,[3] and Y. Otsuka[3]

Received 5 July 2010; revised 24 September 2010; accepted 15 November 2010; published 15 January 2011.

[1] A statistics of motion of polar cap arcs is conducted by using 5 years of optical data from an all-sky imager at Resolute Bay, Canada (74.73°N, 265.07°E). We identified 743 arcs by using an automated arc detection algorithm and statistically examined their moving velocities as estimated by the method of Hosokawa et al. (2006). The number of the arcs studied is about 5 times larger than that in the previous statistics of polar cap arcs by Valladares et al. (1994); thus, we could expect to obtain more statistically significant results. Polar cap arcs are found to fall into two distinct categories: the B_y-dependent and B_y-independent arcs. The motion of the former arcs follows the rule reported by Valladares et al. (1994), who showed that stable polar cap arcs move in the direction of the interplanetary magnetic field (IMF) B_y. About two thirds of the arcs during northward IMF conditions belong to this category. The latter arcs always move poleward irrespective of the sign of the IMF B_y, which possibly correspond to the poleward moving arcs in the morning side reported by Shiokawa et al. (1997). At least one third of the arcs belong to this category. The B_y-dependent arcs tend to move faster when the magnitude of the IMF B_y is larger, suggesting that the transport of open flux by lobe reconnection from one polar cap compartment to the other controls their motion. In contrast, the speed of the B_y-independent arcs does not correlate with the magnitude of the B_y. The motions of both the B_y-dependent and B_y-independent arcs are most probably caused by the magnetospheric convection. Convection in the region of B_y-dependent arcs is affected by the IMF B_y, which indicates that their sources may be on open field lines or in the closed magnetosphere adjacent to the open-closed boundary, whereas B_y-independent arcs seem to be well on closed field lines. Hence, the magnetospheric source of the two types of arc may be different. This implies that the mechanisms causing the motion and generation of arcs could be different between the two types of polar cap arc.

Citation: Hosokawa, K., J. I. Moen, K. Shiokawa, and Y. Otsuka (2011), Motion of polar cap arcs, *J. Geophys. Res.*, *116*, A01305, doi:10.1029/2010JA015906.

1. Introduction

[2] Polar cap arcs are one of the outstanding phenomena in the polar cap during periods of northward interplanetary magnetic field (IMF) [e.g., *Zhu et al.*, 1997, and references therein]. They appear at much higher magnetic latitudes than the auroral features observed during periods of southward IMF. Some arcs cross the entire polar cap from the nightside to the dayside and form a pattern that resembles the Greek letter θ. Such a type of large-scale polar cap arc is called "transpolar arcs" or "θ aurora" [*Frank et al.*, 1986]. Other arcs are relatively shorter in length and tend to occur either in the duskside or dawnside of the polar cap [*Valladares et al.*, 1994]. Such smaller-scale arcs are generally aligned with the noon-midnight meridian; thus, we often call them as "Sun-aligned arcs." Studies of polar cap arcs are quite important since their behavior possibly represents spatial/temporal evolution of the plasma structure in the interaction region between the solar wind and magnetosphere [*Lundin et al.*, 1991]. It is of particular importance to investigate motion of polar cap arcs because it must indicate dynamical characteristics of their source plasma at the magnetospheric altitude.

[3] Optical measurements with ground-based all-sky imagers have been used to visualize the 2D structure of polar cap arcs, which has enabled us to derive the motion of polar cap arcs by examining consecutive all-sky images [e.g., *Valladares et al.*, 1994; *Shiokawa et al.*, 1995]. *Valladares et al.* [1994] employed a large database obtained by all-sky image-intensified photometers located in Qaanaaq, Greenland (77.5°N, 69.2°W) and examined motion of 143 Sun-aligned arcs in 630.0 nm all-sky images. They showed that the dawn-dusk motion of slowly moving stable polar cap arcs is strictly controlled by the sign of the upstream IMF B_y. They interpreted the motion of these B_y-dependent arcs in terms of newly opened fluxes that enter the polar cap and cause a displacement of the convection cells. Later,

[1]Department of Communication Engineering and Informatics, University of Electro-Communications, Tokyo, Japan.
[2]Department of Physics, University of Oslo, Oslo, Norway.
[3]Solar-Terrestrial Environment Laboratory, Nagoya University, Nagoya, Japan.

Copyright 2011 by the American Geophysical Union.
0148-0227/11/2010JA015906

Milan et al. [2005] examined a transpolar arc observed by the IMAGE satellite FUV instrument together with the convection map derived from SuperDARN and proposed a model in which the B_y-dependent motion of polar cap arc is caused by the lobe reconnection through a transport of open flux from one polar cap compartment to the other.

[4] As mentioned above, the B_y-dependent dawn-dusk motion of the stable polar cap arcs was well investigated by *Valladares et al.* [1994] and the mechanism causing such a motion may be explained by the open flux transport between the two bifurcated polar cap compartments [*Milan et al.*, 2005]. However, there exists another class of polar cap arc whose motion is not likely to correlate with the IMF B_y. Such arcs were first reported by *Shiokawa et al.* [1995] who showed that some polar cap arcs in the morning side move poleward repeatedly irrespective of the sign of the IMF B_y. These B_y-independent arcs appear during periods of northward IMF as rayed multiple arcs and most of them occur around the end of substorm-like activities [*Shiokawa et al.*, 1996, 1997]. Later, *Kozlovsky et al.* [2007] suggested that such a type of morning side arc is generated through an interchange instability process occurring between the plasma sheet and the low-latitude boundary layer (LLBL) in the dawn flank of the magnetosphere.

[5] In order to gain more comprehensive understanding of polar cap arcs, we have to differentiate the above mentioned two classes of polar cap arcs, B_y-dependent and B_y-independent arcs, more clearly and discuss their magnetospheric source region separately. For this purpose, it is highly desirable to investigate the motion of polar cap arcs, especially its dependence on the upstream IMF orientation, in a statistical fashion. However, it has been difficult to investigate the motion of polar cap arcs from optical observations statistically. To date, the study by *Valladares et al.* [1994] has been the only one statistical analysis using a large data set sufficient for deriving statistically significant result. A major obstacle to conducting such a research is a difficulty involved in computing the motion of polar cap arcs from a huge amount of optical images automatically. Actually, *Valladares et al.* [1994] only investigated slowly moving stable arcs because they picked up the arcs and estimated their motion manually. Clearly, some automated procedure for extracting the motion of polar cap arcs from a large amount of all-sky images is required to investigate the behavior of polar cap arcs in further detail.

[6] Recently, *Hosokawa et al.* [2006] developed a method for estimating motion of polar cap patches [*Crowley*, 1996] from routine all-sky airglow measurement at Resolute Bay, Canada. This method is based on 2D cross correlation analysis of consecutive all-sky images. *Hosokawa et al.* [2009b] applied this method to the all-sky images obtained at Resolute Bay and carried out a statistical analysis of patch motion. In this paper, we employ the patch-tracking algorithm of *Hosokawa et al.* [2006] to estimate the motion of polar cap arcs. In addition, we newly developed an additional algorithm of automated detection of polar cap arcs. By combining these two methods, we investigate the dawn-dusk motion of polar cap arcs in a statistical fashion. Outline of the paper is as follows: section 2 briefly describes the optical instrument used in the statistical analysis. Section 3 presents the methodology employed to detect the occurrence of polar cap arcs and to compute their motion. In section 4 we introduce the statistical results, and then discuss the motion of polar cap arcs and its dependence on the upstream IMF orientation. Section 5 provides summary of this paper.

2. Instrumentation

[7] An all-sky airglow imager employed in the current statistical analysis was developed by the Solar-Terrestrial Environment Laboratory, Nagoya University, as a part of the Optical Mesosphere Thermosphere Imagers (OMTIs) [*Shiokawa et al.*, 1999]. The OMTI system has been employed to visualize wide varieties of thermospheric phenomena in the midlatitude and low-latitude regions such as traveling ionospheric disturbances, plasma bubbles and low-latitude aurora. The imager at Resolute Bay, Canada (74.73°N, 265.07°E; AACGM latitude 82.9°) has been in operation since January 2005 as a part of the OMTIs system [*Hosokawa et al.*, 2006]. This imager has a number of optical filters, such as 557.7 nm, 630.0 nm, 777.4 nm, Na-line, and OH-band; this enables us to study various upper atmospheric phenomena occurring in the polar cap region, such as polar cap patches [*Hosokawa et al.*, 2006, 2009a, 2009b, 2010a], tongue of ionization [*Hosokawa et al.*, 2009c, 2010b], polar cap aurora [*Koustov et al.*, 2008; *Jayachandran et al.*, 2009], and gravity waves at mesospheric heights [*Suzuki et al.*, 2009].

[8] In the present analysis, all-sky airglow images at a wavelength of 630.0 nm (OI, emission altitude ranges from 200 to 300 km), which are obtained every 2 min with an exposure time of 30 s, are employed for estimating the moving velocities of polar cap arcs. The all-sky observations of the 630.0 nm emission cover the magnetic latitudes from 76° to 90° if we assume the emission height of 250 km. Additionally, time series of the optical intensities at wavelengths of 630.0 nm and 577.7 nm measured at the zenith are used for the automated extraction of arc appearance. Note that the observation at 557.7 nm is absent every 20 min because the background continuum emission (572.5 nm) has to be sampled at these times in order to derive the absolute optical intensity [*Shiokawa et al.*, 2000, 2009]. The imager is operational from September to March, when the Sun and the Moon are sufficiently below the horizon. The data of 5 years, from January 2005 to December 2009, are statistically analyzed in the current study.

3. Method of Statistics

[9] Figure 1 shows three examples of polar cap arc on 2 January 2006, appearing in the dusk (Figure 1a), midnight (Figure 1b), and dawn (Figure 1c) sectors. In these plots, the original 630.0 nm all-sky images have been converted into altitude adjusted corrected geomagnetic (AACGM) coordinates [*Baker and Wing*, 1989] assuming an emission height of 250 km and then mapped in coordinates of magnetic local time (MLT) and magnetic latitude (MLAT). The magnetic midnight is to the bottom and the dotted circle represents MLAT of 80°. Here, the absolute optical intensities are gray-scaled in units of Rayleigh. In all panels, elongated bright emissions, aligned roughly with the Sun-Earth direction, are seen near the zenith of the field-of-view (FOV). Note that other prominent structures in the equatorward part of

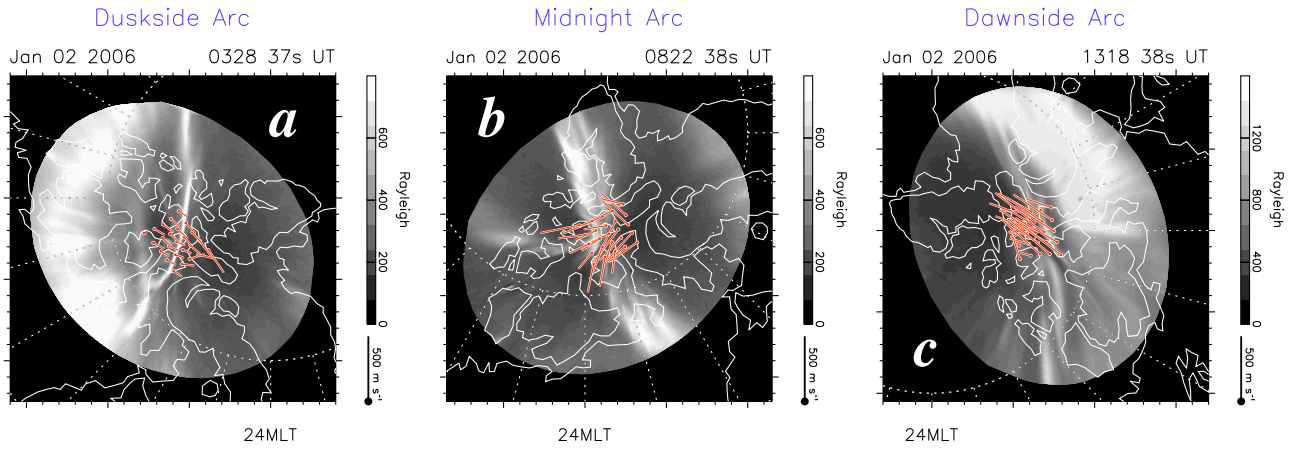

Figure 1. Snapshots of all-sky 630 nm airglow observations of polar cap arcs at (a) 0328 UT, (b) 0822 UT, and (c) 1318 UT on 2 January 2006, which correspond to the duskside, midnight, and dawnside arcs, respectively. The all-sky images are mapped in MLT/MLAT, and the absolute airglow intensity is displayed in units of Rayleigh. Magnetic midnight is to the bottom, and the dotted circle represents MLAT of 80°. The field-of-view of the imager is mapped assuming that height of optical emission is 250 km. Estimated moving vectors of the arcs are overplotted as the red arrows around the zenith.

the Figures 1a and 1c correspond to the poleward portion of the main auroral oval. Moving velocity vectors of these polar cap arcs as estimated by the method of *Hosokawa et al.* [2006] at the 25 points around the zenith are superimposed on the images. The estimated moving velocities are directed almost perpendicular to the alignment of the arcs. The sequences of all-sky images during these intervals (not shown) demonstrate that the estimated motion vectors well trace the bulk motion of the arcs. It should be mentioned that, however, there is a case in which the velocity estimation is somewhat affected by bright auroral features moving along arcs. If an arc has some offset angle with respect to noon-midnight meridian [*Valladares et al.*, 1994], this may contribute to the dawn-dusk velocity component. Although the estimated velocity represents the bulk motion of arcs in most cases, the current statistical analysis using the method of *Hosokawa et al.* [2006] contains some uncertainties associated with the fast motion of arc's substructures.

[10] As shown in Figure 1, the method of *Hosokawa et al.* [2006] tracks the bulk motion of polar cap arcs quite well. However, it is important to note that since cross correlation analysis is based on the optical data that is obtained in the vicinity of the zenith, the derived motion vectors cannot represent an actual motion of arcs unless they are at the zenith. In such a case, the derived vectors should not be used in the current statistical analysis. During extended intervals of northward IMF B_z, polar cap arcs dominate the polar cap region [*Valladares et al.*, 1994] and, in most cases, are observed almost continuously within the FOV of the all-sky imager. However, when the IMF B_z is directed southward, polar cap patches, the other prominent phenomenon occurring in the polar cap region, dominate the polar cap [e.g., *Hosokawa et al.*, 2009b]. The purpose of this study is to examine the motion of polar cap arcs. Thus, it is necessary to first distinguish arcs from patches and to then process the obtained velocities of the polar cap arcs when they are located around the zenith. For this purpose, we developed a method for automatically detecting the occurrence of polar cap arcs from the time series of optical data obtained at the zenith.

[11] Figure 2 describes how the appearance of polar cap arcs at the zenith can be detected automatically. The interval considered here is between 0200 and 1400 UT on 2 January 2006. Figure 2a shows the IMF B_z at the bow shock obtained from the 1 min high-resolution OMNI database (http://omniweb.gsfc.nasa.gov). Except for brief excursions to negative values at around 0400 UT, 0430 UT, 0540 UT and 0720 UT, the IMF B_z was predominantly positive throughout the observation period, representing favorable condition for the occurrence of polar cap arcs [*Valladares et al.*, 1994]. Figures 2b and 2c show the south–north keograms created from 630.0 nm and 577.7 nm airglow images, respectively. The horizontal dashed line corresponds to the zenith. Here, the absolute optical intensities are displayed in units of Rayleigh. The instances of absent 557.7 nm observations are masked with gray lines in Figure 2c. On this day, polar cap arcs did not always appear in the FOV of the imager. They occurred mostly at around 0400 UT, 0800 UT, and 1300 UT, which are corresponding to the duskside, midnight, and dawnside arcs, respectively. During these intervals, stable auroral features always existed at the equatorward edge of the keograms, which probably corresponded to the poleward boundary of the main auroral oval. In the dusk and dawn sectors, a number of signatures of polar cap arcs are identified in both keograms as slanted bright traces, maximum of their optical intensity being around 1 kR. It is clearly seen that most of the arcs were detached from the poleward edge of the main oval and drifted northward. This northward drift corresponds to the dawnward (duskward) motion of the duskside (dawnside) arcs. In contrast, motion of the arc in the midnight sector was not clear. This is probably because the arc in the midnight sector moved almost perpendicular to the cross section of the keograms.

[12] Figures 2d and 2e show the time series of 630.0 nm and 557.7 nm, respectively, emission intensities measured at

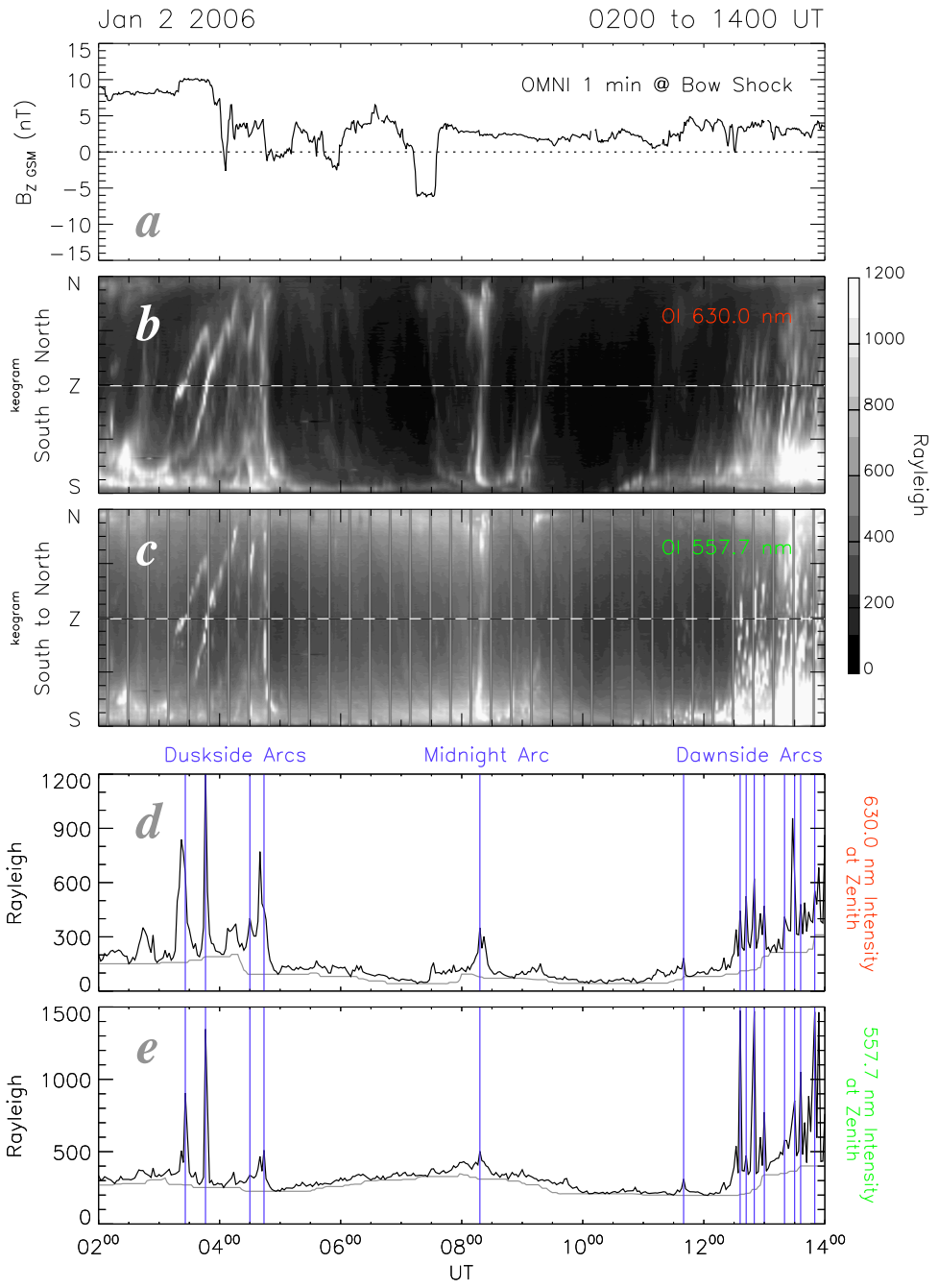

Figure 2. (a) IMF B_z at the bow shock obtained from the 1 min high-resolution OMNI database during 12 h interval from 0200 UT to 1400 UT on 2 January 2006. (b) North–south keogram of 630.0 nm all-sky images. The horizontal dashed line indicates the zenith of the all-sky imager. (c) North–south keogram of 557.7 nm all-sky images. (d) Time series of 630.0 nm emission intensity at the zenith of the all-sky imager. The vertical blue lines mark the times when the centers of polar cap arcs are located at the zenith. The superimposed gray line indicates a baseline estimated by smoothing the local minimums within a 1 h-running window, which represents a possible diurnal variation in the airglow intensity. (e) Time series of 557.7 nm emission intensity at the zenith of the all-sky imager.

the zenith as a black line. The data gaps in 557.7 nm observation, which occurred every 20 min, are linearly interpolated in the time series. The superimposed gray line indicates a baseline estimated by smoothing the local minimums within a 1 h running window, which represents a possible diurnal variation in the airglow intensity. To identify and extract instances of polar cap arc occurrence, we search the data points in the time series sequentially. During this sequential examination, we define a search window of duration 8 min surrounding the data point currently being considered. Then,

we select the data point as an instance of arc occurrence if both the following two conditions are satisfied: (1) the 557.7 nm emission intensity at the current data point is the highest within the window, and (2) the 557.7 nm emission intensity is higher than the baseline by 100 R. In addition to these criteria, we checked the sky conditions every 1 h and only considered the data obtained in good weather conditions.

[13] The polar cap arcs that were detected using this procedure are indicated by the vertical blue lines in Figures 2d and 2e. Fourteen individual arcs were detected in this interval, most of which had a clear counterpart in the keograms shown in Figures 2b and 2c. However, the number of arcs listed is likely to be slightly less than the number of arc signatures seen in Figures 2b and 2c. For example, only one arc was detected in the midnight sector although there were a few tiny peaks in the 557.7 nm emission between 0700 and 1000 UT. This is mainly due to the optical intensity threshold used in the criterion (2) is too large. This criteria was employed for preventing polar cap patches, whose emissions are prominent in both 557.7 nm and 630.0 nm observations, from being identified as polar cap arcs. In the absence of this criterion, the number of the detected arcs would have been double. However, incorrect identification of patches as arcs would considerably contaminate the statistical results; therefore, we processed the data using these selection criteria. The other thing that we must care about is a possible contamination of the dayside transient events such as poleward moving auroral forms (PMAFs) [*Moen et al.*, 1995; *Sandholt et al.*, 1998] and reversed flow events (RFEs) [*Moen et al.*, 2008]. However, the all-sky imager at Resolute Bay is not operative in daylight between 08–14 MLT during which the above mentioned dayside transient events are frequently observed [e.g., *Provan and Yeoman*, 1999; *Rinne et al.*, 2007]; thus, any special care does not need to be taken. We applied the above algorithm to all available optical images obtained from 14 to 08 MLT. Consequently, 743 individual polar cap arcs were identified in total, which is about 5 times larger than the number of arcs examined by *Valladares et al.* [1994].

4. Results and Discussion

[14] For the 743 individual polar cap arcs extracted in section 3, their moving velocities estimated by the method of *Hosokawa et al.* [2006] were examined statistically. We only employ the velocity estimates at the zenith in the statistical analysis although all of the estimated velocities surrounding the zenith are displayed in Figure 1. In particular, the relationship between the duskward velocity of the arcs and the upstream IMF orientations is discussed here in detail. To compare the arc velocities with the IMF parameters, we used the 1 min high-resolution OMNI data to obtain the IMF values at the bow shock. The 1 min high-resolution OMNI database use the magnetic field data obtained by the ACE, WIND, IMP-8 and Geotail satellites. The solar wind propagation time is calculated by using the solar wind velocities observed by these satellites. Detail of the 1 min high-resolution OMNI database can be found in http://omniweb.gsfc.nasa.gov/html/HROdocum.html. An additional time shift of 22 min was considered to account for the delay from the dayside bow shock to the near-midnight part of the polar cap ionosphere. The reason why we decided to use the time delay of 22 min in the statistics will be discussed in the later part of this section. Furthermore, since most of the arcs stay around the zenith for at least about 10 min, our velocity estimation with a temporal resolution of 2 min would introduce multiple velocity data for a single arc. Thus, we considered all the velocity data within the 8 min search window around the time when the arc was located exactly at the zenith. This procedure can increase the number of data points in the statistics and would hence increase the significance of the statistical distributions.

[15] Before discussing the dependence of the arc motion on the IMF, we briefly show how the occurrence of polar cap arcs depends on the IMF orientation. Figure 3a shows the occurrence distribution of the 743 polar cap arcs as a function of the IMF clock angle(CA). The distribution is rather symmetric about the CA = 180° line. It is also clearly seen that most of the arcs (≈70 %) were observed when the IMF was directed northward ($0° < CA < 90°$ and $270° < CA < 360°$). Early studies by *Berkey et al.* [1976] and *Lassen and Danielsen* [1978] found good correlation between IMF B_z northward conditions and appearance of polar cap arcs. Our statistical results are basically consistent with their earlier finding. However, it should be noted that 30% of the arcs were observed during the southward IMF conditions ($90° < CA < 270°$). *Valladares et al.* [1994] also pointed out that polar cap arcs are sometimes seen during intervals of southward IMF. Actually, about 20 % of the polar cap arcs in their statistical analysis were observed during the southward IMF conditions although the probability decreased as the IMF B_z became more negative. They claimed that the polar cap arcs appearing in the southward IMF conditions originated before the IMF B_z turned from positive to negative and remained observable for a while after the polarity change of IMF B_z. Thus, we consider that the data points during the southward IMF conditions are not associated with misidentification of patches as arcs.

[16] Now we turn to discuss the main topic of this paper; the relationship between the arc motion in the dawn-dusk direction and the IMF orientation. Figure 3b shows the distribution of the duskward velocity of the arcs as a function of the IMF CA, in which velocity data estimated for all of the arcs between 14 and 08 MLT are used. The gray scale demonstrates the density of data points in percentage on a linear scale, self-normalized. To aid the discussion, we divide the plot area into eight regions from Region I to VIII according to the sign of the duskward velocity and the IMF CA. The occurrence percentage of the arcs is computed for each region and plotted together. Although there are lots of data points during the southward IMF period (in Regions II, III, VI, and VII), we focus our attention on the motion of the arcs during the northward IMF conditions (Regions I, IV, V, and VIII). The occurrence is clearly found to be higher in Region I (25.3 %) and Region VIII (19.8 %). In these regions indicated by the blue rectangles, the arcs move duskward (dawnward) when the IMF B_y is directed eastward (westward). This systematic behavior is obviously consistent with the rule reported by *Valladares et al.* [1994] who showed that most of the stable polar cap arcs move in the direction of the IMF B_y. Thus, about 65 % of the polar cap arcs during the northward IMF, (25.3 % + 19.8 %) / 70 %, can be categorized as the stable B_y-dependent arcs reported by *Valladares et al.* [1994].

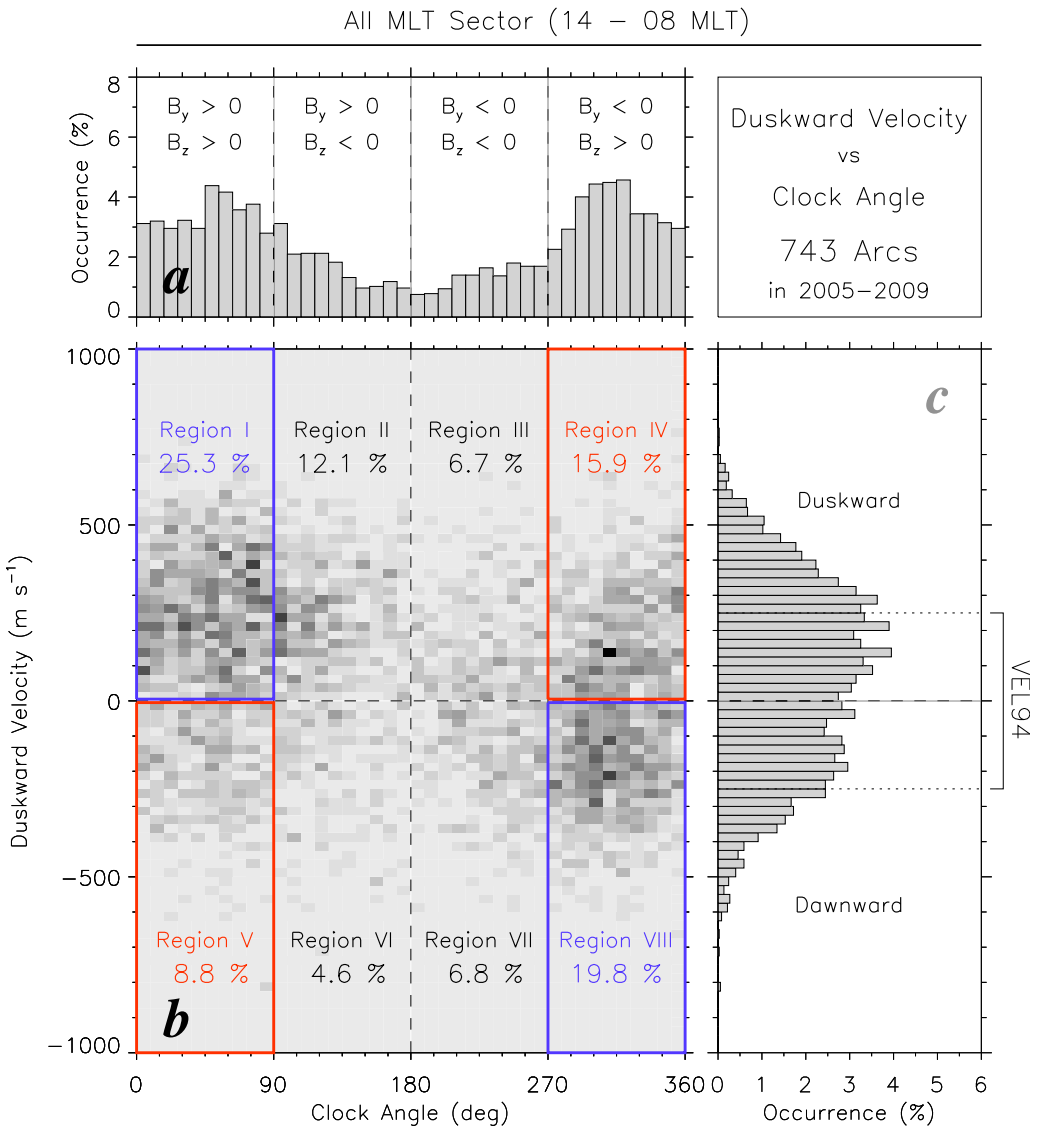

Figure 3. (a) Occurrence distribution of the polar cap arcs as a function of the IMF clock angle. (b) Occurrence distribution of the duskward velocity of the arcs as a function of the IMF clock angle. The gray scale shows the density of data points in percentage on a linear scale, self-normalized. To aid discussion, we divide the plot area into eight regions from Region I to VIII according to the sign of the duskward velocity and IMF orientation. (c) Occurrence distribution of the duskward velocity of the arc.

[17] Although the dawn-dusk motion of 65 % of the arcs is found to follow the rule of *Valladares et al.* [1994], there exist other populations whose dawn-dusk motion looks independent on the sign of IMF B_y. Such populations can be seen in Regions IV (15.9 %) and V (8.8 %), which are indicated by the red rectangles in Figure 3b. The arcs in these regions move duskward (dawnward) when the IMF B_y is directed westward (eastward). *Valladares et al.* [1994] also showed that the dawn-dusk motion of the polar cap arcs depends not only on B_y sign but also on the location of the arcs within the polar cap. They suggested that there exist two cells on the duskside and dawnside, in which arcs always move dawnward and duskward, respectively. For IMF $B_y < 0$, the dusk cell is larger, so that the arcs seen near the pole move dawnward. For $B_y > 0$, the dawn cell is larger, thus, duskward motion is observed near the pole. However, for any B_y sign there are poleward moving arcs at somewhat lower latitude in both dawn and dusk sectors. Perhaps, these arcs are classified as the B_y-independent arcs seen in the current statistics. In Figure 3b, we employ all the data point obtained between 14 and 08 MLT; thus we cannot exactly see where these B_y-independent arcs came from. In order to clarify the behavior of such arcs in more detail, we will investigate the distribution of the arc velocities in three separate MLT sectors (duskside, midnight, and dawnside) individually in the later part of this section.

[18] In Figure 3c, the distribution of the duskward velocity is shown. The distribution is rather broad, ranging from –600 m s^{-1} to 600 m s^{-1} although maximum occurrence is located at around 100–200 m s^{-1}. As mentioned in section 1,

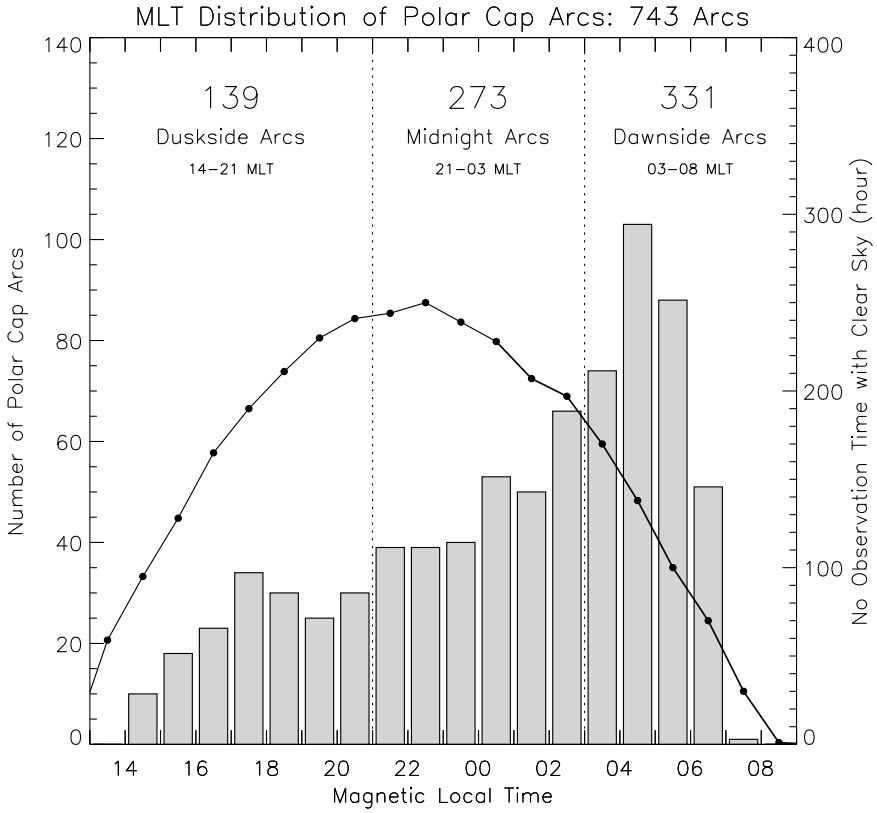

Figure 4. The MLT distribution of the 743 polar cap arcs. Also superimposed is the distribution of the number of observation hours with a clear-sky condition.

the study of *Valladares et al.* [1994] only investigated the dawn-dusk motion of slowly moving stable polar cap arcs whose duskward speed is less than 250 m s^{-1}. This velocity limitation of 250 m s^{-1} is overplotted as the horizontal dotted lines for comparison (VEL94). This limitation is probably due to the fact that they derived the motion of arcs by fitting their structure in consecutive images manually. In contrast, we computed the motion of arcs automatically; thus, polar cap arcs moving with relatively higher speed can be included in the current statistics. Our statistical result demonstrates an existence of high-speed arcs whose duskward speed is well greater than 250 m s^{-1}. Such high-speed arcs were actually observed by some of the previous works [e.g., *Shiokawa et al.*, 1995, 1996, 1997; *Kozlovsky et al.*, 2003, 2007]; thus, they could be a significant component of polar cap arcs.

[19] Now we turn to investigate the distribution of the duskward velocities in three separate MLT sectors (duskside, midnight, and dawnside) individually. Figure 4 shows the MLT distribution of the 743 polar cap arcs as a histogram. Also superimposed is the distribution of the number of observation hours with a clear-sky condition (black line). The occurrence distribution of the arcs is rather asymmetric and occurrence rate is clearly higher in the dawn sector than in the dusk sector, maximum being around 05 MLT. Note that less occurrence of the arcs in the evening sector is not due to a bad weather condition in that local time sector. This is consistent with the results of *Valladares et al.* [1994] who pointed out that the occurrence of stable polar cap arcs is 4 times larger in the dawnside than in the duskside. Another important point is that the MLT distribution of the polar cap arc is quite different from that of polar cap patches, which typically forms a bell shaped symmetric distribution whose center is around 23 MLT [e.g., *Moen et al.*, 2007]. This again suggests that the automated detection described above works very well in distinguishing polar cap arcs from patches. In order to investigate the distribution of the arc velocities in separate MLT sectors individually, we sort the arcs into three categories, duskside arcs (14–21 MLT), midnight arcs (21–03 MLT), and dawnside arcs (03–08 MLT). The number of the duskside, midnight, and dawnside arcs is 139, 273, and 331, respectively.

[20] Figure 5 again shows the distribution of the duskward velocity of the duskside arcs (Figure 5, left), midnight arcs (Figure 5, middle), and dawnside arcs (Figure 5, right) as a function of the IMF CA. In all MLT sectors, an existence of the B_y-dependent arcs is obvious in the regions indicated by the blue rectangles. About two thirds of the polar cap arcs during the northward IMF conditions follow the rule of *Valladares et al.* [1994] and move back and forth in the dawn-dusk direction in close association with change of the sign in the IMF B_y. However, if we look at the distributions in the dusk and dawn sectors, we can identify populations, which always move poleward irrespective of the sign of IMF B_y (as indicated by the red rectangles). In the dusk sector, the arcs in Region V (21.8 %) appear to move dawnward (i.e., poleward in this local time sector) even when the IMF B_y is directed eastward. Also in the dawn sector, an existence

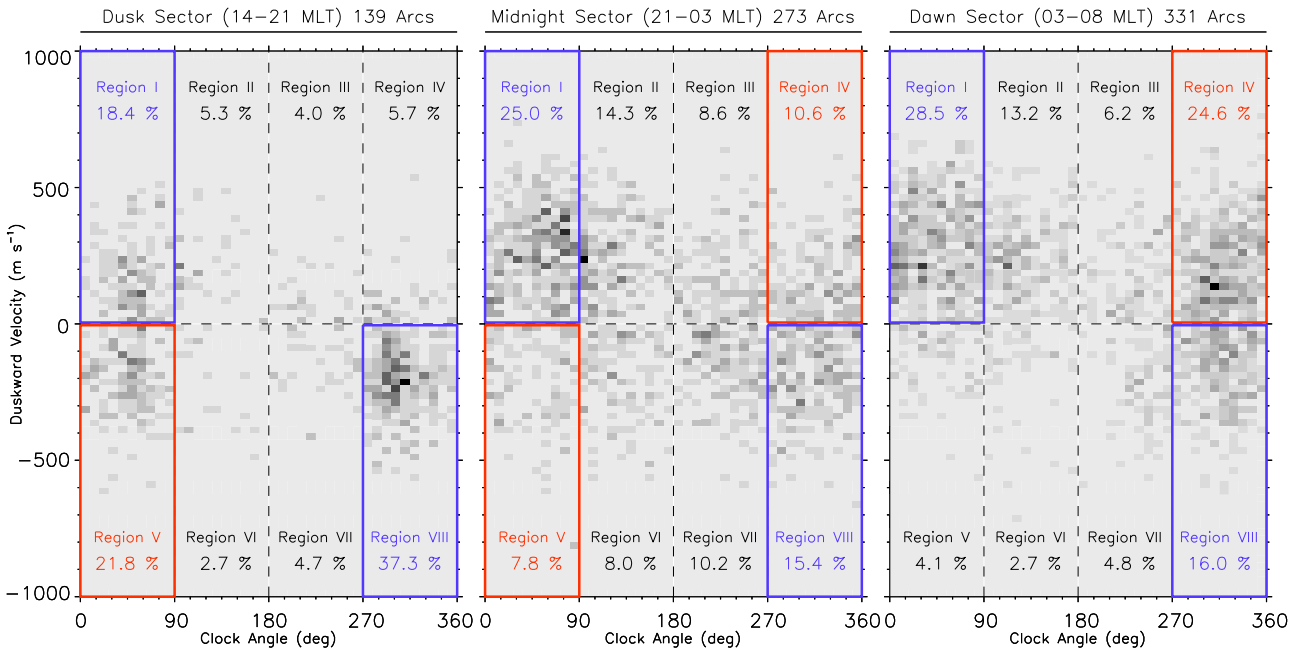

Figure 5. Occurrence distribution of the duskward velocity of the polar cap arcs as a function of the IMF clock angle for the arcs in the (left) duskside (14–21 MLT), (middle) midnight (21–03 MLT), and (right) dawnside (03–08 MLT).

of the B_y-independent arcs can be identified in Region IV (24.6 %), in which arcs move duskward (i.e., poleward in this local time sector) even if the IMF B_y is directed westward.

[21] The B_y-independent arcs in Region IV in the dawn sector possibly correspond to the poleward moving arcs reported by *Shiokawa et al.* [1995, 1996, 1997]. In their studies, such poleward moving arcs were investigated only in the morning side local time sector. However, the current statistics demonstrates that the poleward moving arcs appear also in the dusk sector although their occurrence rate is slightly smaller. *Shiokawa et al.* [1995] showed that most of the polar cap arcs in the morning side move poleward for both positive and negative IMF B_y conditions. Thus, Region VIII in the dusk sector (37.3 %) and Region I in the dawn sector (28.5 %) would also contain some of the B_y-independent poleward moving arcs. Thus, perhaps more than one third of the polar cap arcs move poleward irrespective of the sign of the IMF B_y.

[22] In Figure 5 (middle), the distribution of the duskward velocity of the midnight arcs is shown. Again, we can identify an occurrence of both the B_y-dependent and B_y-independent arcs, which are indicated by the blue and red rectangles, respectively. Interestingly, the occurrence percentage of the B_y-independent arcs is clearly smaller than that in the dusk and dawn sector. *Shiokawa et al.* [1995] reported that almost all of the poleward moving arcs in the morning side local time sector tend to disappear at a certain latitude around 85° MLAT before entering the midnight sector. This could be a reason why the B_y-independent arcs are less prominent in the midnight sector. In contrast, the occurrence of the B_y-dependent arcs remains high in the midnight sector (25.4 % in Region I and 15.4 % in Region VIII) suggesting that the B_y-dependent arcs originating either from dusk or dawn sector can travel for long distance across the midnight polar cap area if the IMF B_y is in a favorable direction for their transpolar cap motion. This contrast between the two types of polar cap arc again suggests that the source of the B_y-dependent and B_y-independent arcs is different.

[23] Figure 6 summarizes the motion of the two types of polar cap arc for positive (Figure 6, left) and negative (Figure 6, right) IMF B_y conditions. Here, the structure of the arcs is drawn as their bottom edge is directly connected to the poleward edge of the main auroral oval. However, the FOV of the all-sky camera is too narrow to confirm the spatial relationship between the polar cap arcs and poleward edge of the main oval. Probably, this is the case at least for the B_y-dependent arcs since large-scale polar cap arcs such as θ aurora observed by the space-based global auroral imager generally connect to the main oval on one side or both sides [e.g., *Kullen et al.*, 2002]. For the B_y-independent arcs, however, *Shiokawa et al.* [1996] mentioned that the morning side poleward moving arcs were detached from the stable equatorward aurora; thus, the structure of the B_y-independent arcs may be detached completely from the main auroral oval. In Figure 6, the blue (red) arrows show the direction of the motion of the B_y-dependent (B_y-independent) arcs. The sizes of the arrows indicate the approximate fractions of the numbers of arcs. As mentioned above, the B_y-dependent arcs move in the direction of the IMF B_y and the B_y-independent arcs move poleward irrespective of the sign of the IMF B_y. In the dawn sector, both the B_y-dependent and B_y-independent arcs move poleward when the IMF B_y is positive; thus, we could not differentiate them only from this statistical analysis. The same situation occurs

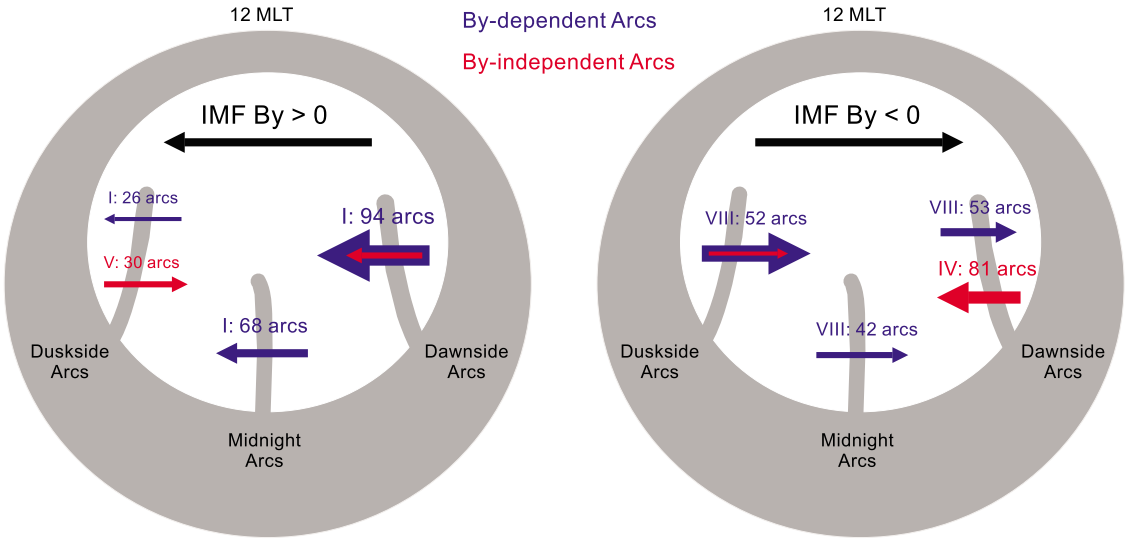

Figure 6. Summary of the motion of polar cap arcs during northward IMF conditions for positive IMF B_y and negative IMF B_y cases. The blue (red) arrows show the motion of the B_y-dependent (B_y-independent) arcs. The sizes of the arrow indicate the approximate fraction of the numbers of arcs.

in the dusk sector when the IMF B_y is negative. In the midnight sector, the B_y-independent arcs are less prominent and B_y-dependent arcs are dominant.

[24] The contrast in the dependence of the motion on the IMF B_y strongly suggests that the mechanism causing the motion of polar cap arc is different between the B_y-dependent and B_y-independent arcs. Here, we try to reveal what controls the motion of the two types of arc by investigating the correlation between the moving speed of the arcs and the magnitude of the IMF B_y. Figure 7 shows how the speed of the arcs in the dawn-dusk direction depends on the magnitude of the IMF B_y. Here, we again employ the time delay of 22 min between the time of the solar wind measurements at the bow shock and that of the optical observations in the central polar cap. In Figure 7a, we plot the moving speed of the B_y-dependent arcs in the dawn-dusk direction as a

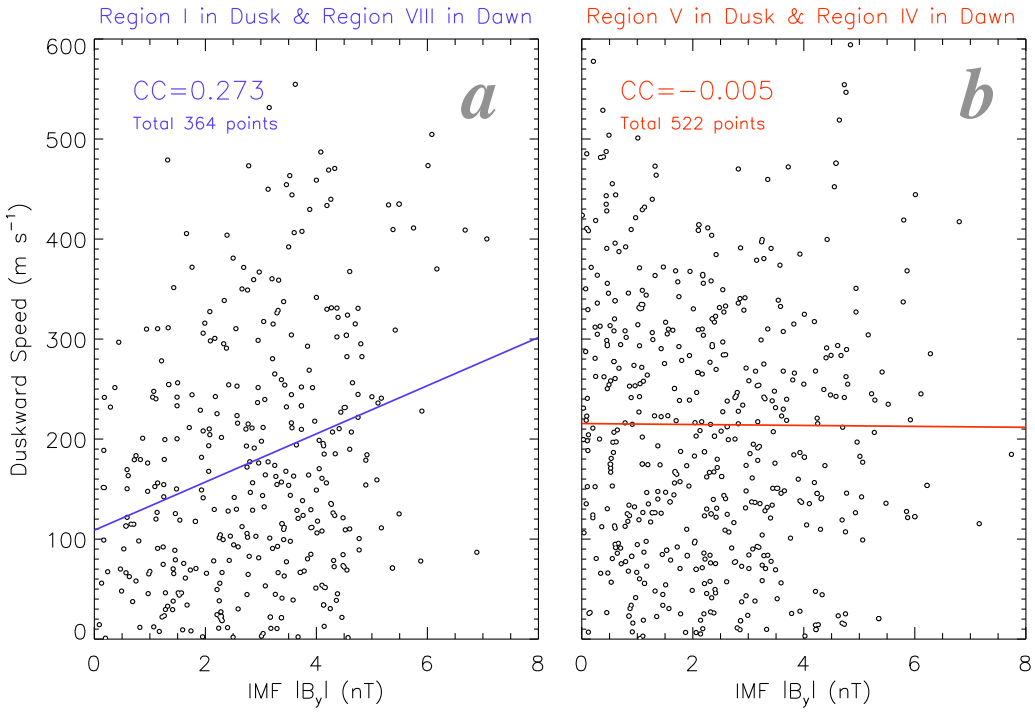

Figure 7. (a) Correlation between the duskward speed of the B_y-dependent arcs and the magnitude of the IMF B_y. (b) Correlation between the duskward speed of the B_y-independent arcs and the magnitude of the IMF B_y.

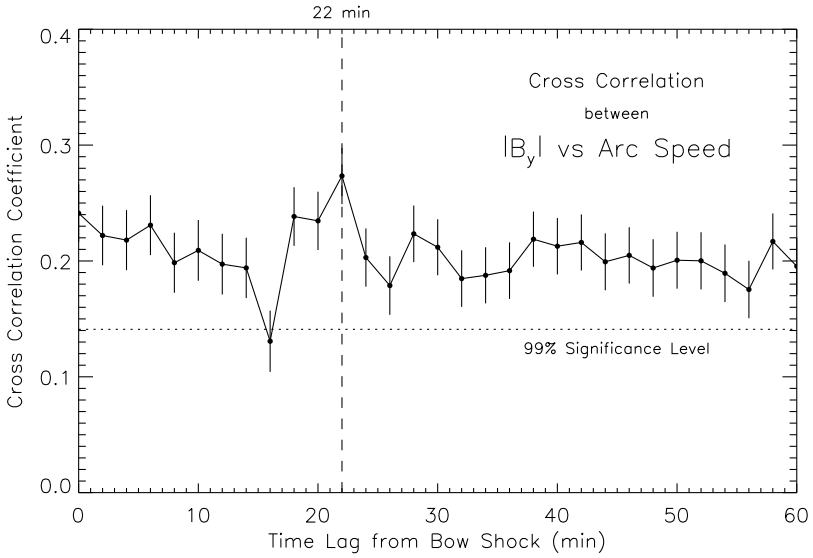

Figure 8. Cross correlation coefficient between the magnitude of the IMF B_y and the duskward speed of the B_y-dependent arcs as a function of time lag from the bow shock. The horizontal dotted line shows the 99 % significance level.

function of the magnitude of the IMF B_y. Here, we plot the data points in Region I in the dusk sector and Region VIII in the dawn sector. In these regions, almost all the data points correspond to the B_y-dependent arcs. It is seen that the speed of the arc motion exhibits a weak positive correlation with the magnitude of the IMF B_y, the correlation coefficient being 0.273. This slight correlation implies that the B_y-dependent arcs move faster when the magnitude of the IMF B_y is larger.

[25] *Milan et al.* [2005] interpreted the motion of transpolar arc, which can be categorized as the B_y-dependent arc, in terms of open flux transport between two polar cap compartments separated by the arc. When the polar cap arc appears during an interval of northward IMF and polar cap (and magnetotail lobe) is divided into two compartments by the arc, the lobe reconnection occurring poleward of the cusp can transport the open flux in one compartment into the other. Such a flux transport can cause the former to contract and the latter to expand. This expansion/contraction of the polar cap compartments causes the arc motion in the direction of the IMF B_y. According to this idea, if the IMF B_y becomes larger, the flux is transported between the two polar cap areas more efficiently and the resulting motion of the arc could be faster. The positive correlation shown in Figure 7a suggests that the process proposed by *Milan et al.* [2005] actually contributes to the motion of the B_y-dependent polar cap arcs.

[26] In Figure 7b, we plot the moving speed of the B_y-independent arcs in the dawn-dusk direction as a function of the magnitude of the IMF B_y. Here, we plot the data points in Region V in the dusk sector and Region IV in the dawn sector. In these regions, almost all the data points correspond to the B_y-independent arcs. In contrast to the B_y-dependent arcs, the moving speed of the B_y-independent arcs does not depend on the magnitude of the IMF B_y, the correlation coefficient being −0.005. This suggests that open flux transport between the separated polar caps does not contribute to the motion of the B_y-independent arcs; thus, the mechanism controlling the motion of the B_y-independent arc is fundamentally different from the process suggested by *Milan et al.* [2005]. This also indicates that during intervals of the B_y-independent arc the magnetotail lobe is not separated into two compartments, implying that the source of the B_y-independent arc is not located in the nightside plasma sheet as suggested by *Frank et al.* [1986].

[27] *Shiokawa et al.* [1996] suggested that the poleward moving arcs in the morning side originate from the boundary region between the plasma sheet and the LLBL in the morning side tail flank. Later, *Shiokawa et al.* [1997] compared their optical observations with a global MHD simulation and claimed that the source of the poleward moving arcs is in the morning side tail flank where the plasmas from the LLBL and from the plasma sheet are mixed. More recently, *Kozlovsky et al.* [2007] proposed a model in which the poleward moving arcs in the morning side are formed through an interchange instability occurring in the dawn flank of the magnetosphere between the plasma sheet plasma coming from the nightside and the magnetosheath flux tubes entering the LLBL from dayside. The absence of the correlation between the speed of the B_y-independent arcs and the magnitude of the IMF B_y shown in Figure 7b supports these ideas.

[28] We also statistically analyzed the correlation between the arc speed and the rate of IMF B_y change. However, it was found that the speed of both types of arc does not depend on the rate of B_y change. For the case of the B_y-dependent arcs, the rate of flux transport between the polar cap compartments separated by polar cap arcs is determined by the IMF B_y-associated azimuthal component of the lobe cell convection, whose strength is basically a function of the reconnection electric field. The reconnection electric field generally depends on the magnitude of the IMF (not the rate of IMF change). This could be the reason why we obtain a higher correlation with the magnitude of IMF B_y rather than the rate of B_y change. We also checked the dependence of

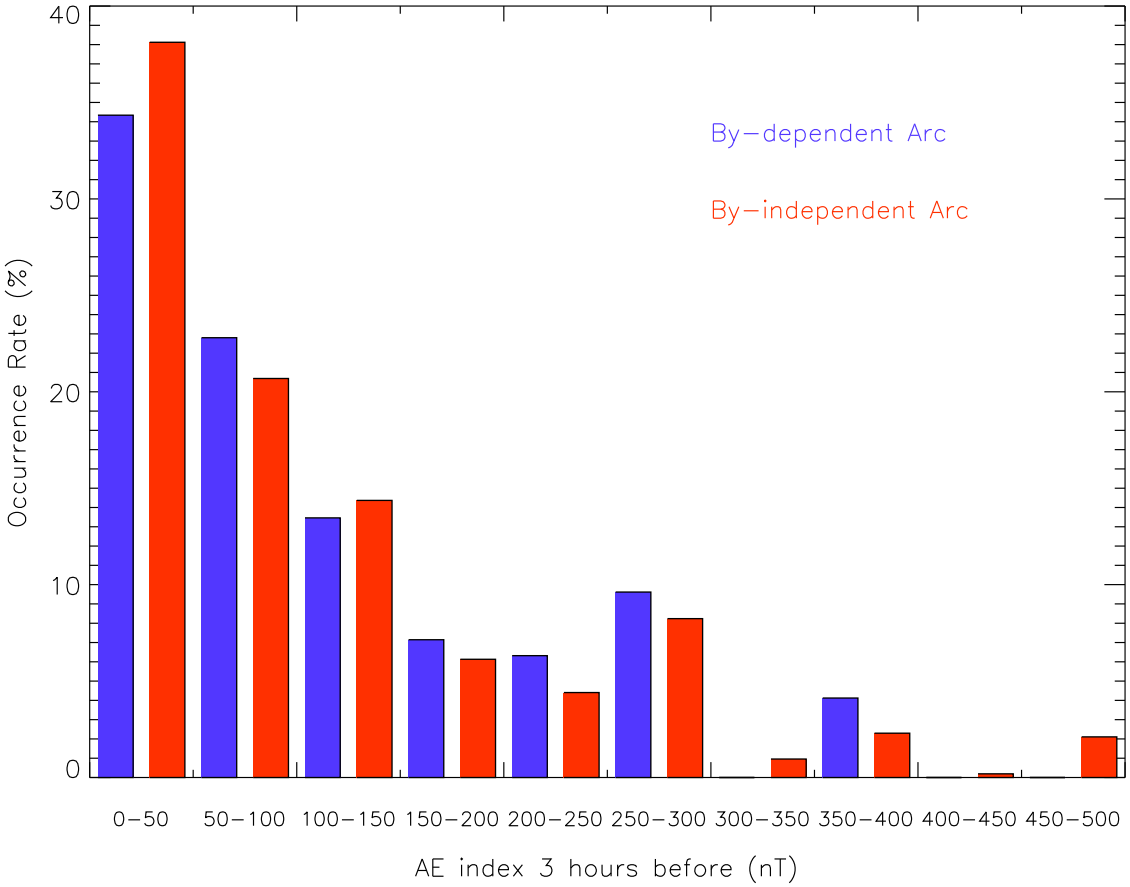

Figure 9. Occurrence distribution of the B_y-dependent (blue) and B_y-independent (red) arcs as a function of the provisional AE index 3 h before their appearance.

the arc speed on the IMF B_x, B_z, solar wind speed and density. However, we could not see any significant difference between the two types of polar cap arc; thus, only the dependence of the arc speed on the IMF B_y can differentiate the B_y-dependent and B_y-independent arcs.

[29] As shown in the Figure 7a, the speed of the B_y-dependent arcs depends on the magnitude of the IMF B_y. By using this relationship we can determine the time needed for the B_y-dependent arcs to respond the variation of the upstream IMF orientations. Figure 8 shows the cross correlation coefficients between the magnitude of the IMF B_y and the duskward speed of the B_y-dependent arcs as a function of time lag from the bow shock. The horizontal dotted line shows the 99 % significance level derived from Student's t-test. The error bars show the standard error of the coefficient, given by $\epsilon = (1 - r^2)/(n - 2)^{1/2}$, where r is the value of the coefficient and n is the number of data points from which it was determined [*Hosokawa et al.*, 2006]. The coefficient between $|B_y|$ and arc speed has a peak at 22 min and the coefficient at the peak is well above the statistical significance level. We cannot exactly determine the solar wind propagation delay from the bow shock to the dayside magnetopause. However, it is typically around 5–10 min. Thus, it takes another 10–15 min for the B_y-dependent arcs to respond to the change of the upstream IMF orientations, which probably corresponds to the time needed for the lobe reconnection to transport the open flux from one polar cap compartment into the other. This delay of 10–15 min is slightly shorter than the value suggested by *Valladares et al.* [1994] who claimed that it would take about 30 min for a solar wind disturbance to travel from the dayside magnetosphere up to the far regions of the magnetotail and affect the motion of polar cap arcs.

[30] *Shiokawa et al.* [1997] showed that most of the morning side poleward moving polar cap arcs occurred around the end of substorm-like magnetic activity, suggesting that the source of the arcs is related to the plasma sheet particles. In order to confirm this characteristics, we investigate the AE index 3 h before the appearance of the B_y-dependent and B_y-independent arcs shown in Figure 7. In Figure 9, we plot the occurrence distribution of the B_y-dependent and B_y-independent arcs as a function of the provisional AE index 3 h before their appearance. Both the B_y-dependent and B_y-independent arcs mostly appeared when the AE index was low. About 70 % of the arcs occurred when the AE index was less than 100 nT. This result is consistent with the fact that the polar cap arcs mostly appear during the northward IMF conditions. More important point to note is that the occurrence rate of the B_y-independent arcs did not always depend on the level of substorm activity before they occurred. Thus, the activation of the plasma sheet particles is not likely to be a necessary condition for the formation of B_y-independent arcs, which is inconsistent with the result of *Shiokawa et al.* [1997].

[31] The current statistical analysis using a huge database of optical observation clearly demonstrated that there exist two distinct classes of polar cap arcs, B_y-dependent and B_y-independent arcs. Several differences were identified between these two types of polar cap arc, which implied that their source and generation mechanism are different. Recently, vast numbers of new instruments have been deployed to the polar cap area in the northern hemisphere for the observation of solar wind driven ionospheric phenomena, e.g., all-sky airglow imagers, GPS receivers, ionosondes, coherent HF radars, and incoherent scatter radar. Coordinated multi-instrument observations, in situ and by remote sensing techniques, across the entire polar cap are needed to fully understand the complex behavior of polar cap arcs and reveal their magnetospheric source.

5. Summary and Conclusion

[32] We conducted a statistical analysis of motion of polar cap arc by using 5 years of optical data obtained by an all-sky airglow imager located in the polar cap region at Resolute Bay, Canada. We identified 743 individual polar cap arcs by developing an automated arc detection algorithm. For the 743 individual polar cap arcs, their moving velocities estimated by the method of *Hosokawa et al.* [2006] were examined statistically. In particular, the relationship between the duskward velocity of the arc and the upstream IMF orientations was examined in detail. The number of the arcs studied is about 5 times larger than that in the previous statistics of polar cap arcs by *Valladares et al.* [1994]; thus, we could expect to obtain more statistically significant results.

[33] Polar cap arcs during northward IMF conditions fall into two distinct categories, the B_y-dependent and B_y-independent arcs. The motion of the former arcs strictly follows the rule reported by *Valladares et al.* [1994] who showed that the slowly moving stable polar cap arcs move in the direction of the IMF B_y. About two thirds of the arcs during northward IMF conditions belong to the category of the B_y-dependent arcs. The latter arcs always move poleward irrespective of the sign of the IMF B_y. These B_y-independent arcs possibly correspond to the poleward moving arcs in the morning side reported by *Shiokawa et al.* [1995, 1996, 1997]. These arcs have been observed near the poleward edge of the morning side auroral oval. However, we identified such poleward moving arcs also in the dusk local time sector. At least (perhaps more than) one third of the arcs during northward IMF conditions belong to the category of the B_y-independent arcs.

[34] It is also demonstrated that the B_y-dependent arcs move faster when the magnitude of the IMF B_y is larger. This implies that transport of open flux by the lobe reconnection from one polar cap compartment to the other controls the motion of the B_y-dependent arcs. In contrast, the moving speed of the B_y-independent arcs does not correlate with the magnitude of the B_y. The motions of both the B_y-dependent and B_y-independent arcs are most probably caused by the magnetospheric convection. Convection in the region of B_y-dependent arcs is affected by the IMF B_y, which indicates that their sources may be on open field lines or in the closed magnetosphere adjacent to the open-closed boundary, whereas B_y-independent arcs seem to be well on closed field lines. Hence, the magnetospheric source of the two types of arc may be different. This implies that the mechanisms causing the motion and generation of arcs could be different between the two types of arcs.

[35] **Acknowledgments.** This work was supported by Grants-in-Aid for Scientific Research (16403007, 19403010, 20244080, and 20740282) from the Japan Society for the Promotion of Science (JSPS). This work was carried out by the joint research program of the Solar-Terrestrial Environment Laboratory (STEL), Nagoya University. The authors thank Y. Katoh, M. Satoh, and T. Katoh of STEL, Nagoya University, for kind support in airglow imaging observations. Special thanks are extended to staff of the Narwhal Arctic Service at Resolute Bay for kind and helpful support in operating the optical instrument. The optical observation at Resolute Bay was also supported by the NSF cooperative agreement ATM-0608577. The provisional AE index was provided by World Data Center (WDC) for Geomagnetism, Kyoto. The OMNI-2 data were obtained from NASA/NSSDC. This work was done while K.H. was staying at the Department of Physics, University of Oslo, as a guest researcher. His research at University of Oslo was supported by a grant of "Excellent Young Researcher Overseas Visit Program" from JSPS. J.M. has been sponsored by the Norwegian Research Council, the AirForce Office of Scientific Research, Air Force Material Command, USAF, under grant FA8655-10-1-3003, and COST action ES0803.

[36] Robert Lysak thanks Alexander Kozlovsky and another reviewer for their assistance in evaluating this paper.

References

Baker, K. B., and S. Wing (1989), A new magnetic coordinate system for conjugate studies of high latitudes, *J. Geophys. Res.*, *94*, 9139–9143, doi:10.1029/JA094iA07p09139.

Berkey, T., L. L. Cogger, S. Ismail, and Y. Kamide (1976), Evidence for a correlation between Sun-aligned arcs and the interplanetary magnetic field direction, *Geophys. Res. Lett.*, *3*, 145–147, doi:10.1029/GL003i003p00145.

Crowley, G. (1996), Critical review of ionospheric patches and blobs, in *Review of Radio Science* 1993–1996, edited by W. R. Stone, p. 619, Oxford Univ. Press, New York.

Frank, L., et al. (1986), The theta aurora, *J. Geophys. Res.*, *91*, 3177–3224.

Hosokawa, K., K. Shiokawa, Y. Otsuka, A. Nakajima, T. Ogawa, and J. D. Kelly (2006), Estimating drift velocity of polar cap patches with all-sky airglow imager at Resolute Bay, Canada, *Geophys. Res. Lett.*, *33*, L15111, doi:10.1029/2006GL026916.

Hosokawa, K., K. Shiokawa, Y. Otsuka, T. Ogawa, J.-P. St-Maurice, G. J. Sofko, and D. A. Andre (2009a), Relationship between polar cap patches and field-aligned irregularities as observed with an all-sky airglow imager at Resolute Bay and the PolarDARN radar at Rankin Inlet, *J. Geophys. Res.*, *114*, A03306, doi:10.1029/2008JA013707.

Hosokawa, K., T. Kashimoto, S. Suzuki, K. Shiokawa, Y. Otsuka, and T. Ogawa (2009b), Motion of polar cap patches: A statistical study with all-sky airglow imager at Resolute Bay, Canada, *J. Geophys. Res.*, *114*, A04318, doi:10.1029/2008JA014020.

Hosokawa, K., T. Tsugawa, K. Shiokawa, Y. Otsuka, T. Ogawa, and M. Hairston (2009c), Unusually elongated, bright airglow plume in the polar cap F region: Is it tongue of ionization?, *Geophys. Res. Lett.*, *36*, L07103, doi:10.1029/2009GL037512.

Hosokawa, K., J.-P. St.-Maurice, G. J. Sofko, K. Shiokawa, Y. Otsuka, and T. Ogawa (2010a), Reorganization of polar cap patches through shears in the background plasma convection, *J. Geophys. Res.*, *115*, A01303, doi:10.1029/2009JA014599.

Hosokawa, K., T. Tsugawa, K. Shiokawa, Y. Otsuka, N. Nishitani, T. Ogawa, M. Hairston, and L. J. Paxton (2010b), Dynamic temporal evolution of polar cap tongue of ionization during magnetic storm, *J. Geophys. Res.*, *115*, A12333, doi:10.1029/2010JA015848.

Jayachandran, P. T., K. Hosokawa, J. W. MacDougall, S. Mushini, R. B. Langley, and K. Shiokawa (2009), GPS total electron content variations associated with a polar cap arc, *J. Geophys. Res.*, *114*, A12304, doi:10.1029/2009JA014916.

Koustov, A., K. Hosokawa, N. Nishitani, T. Ogawa, and K. Shiokawa (2008), Rankin Inlet PolarDARN radar observations of duskward moving Sun-aligned optical forms, *Ann. Geophys.*, *26*, 2711–2723, doi:10.5194/angeo-26-2711-2008.

Kozlovsky, A., V. Safargaleev, J. Jussila, and A. Koustov (2003), Pre-noon high-latitude auroral arcs as a manifestation of the interchange instability, *Ann. Geophys.*, *21*, 2303–2314.

Kozlovsky, A., A. Aikio, T. Turunen, H. Nilsson, T. Sergienko, V. Safargaleev, and K. Kauristie (2007), Dynamics and electric currents of morningside Sun-aligned auroral arcs, *J. Geophys. Res.*, *112*, A06306, doi:10.1029/2006JA012244.

Kullen, A., M. Brittnacher, J. A. Cumnock, and L. G. Blomberg (2002), Solar wind dependence of the occurrence and motion of polar auroral arcs: A statistical study, *J. Geophys. Res.*, *107*(A11), 1362, doi:10.1029/2002JA009245.

Lassen, K., and C. Danielsen (1978), Quiet time pattern of auroral arcs for different directions of the interplanetary magnetic field in the Y-Z plane, *J. Geophys. Res.*, *83*, 5277–5284, doi:10.1029/JA083iA11p05277.

Lundin, R., L. Eliasson, and J. S. Murphree (1991), The quiet time aurora and magnetospheric configuration, in *Auroral Physics*, edited by C.-I. Meng, M. J. Rycroft, and L. A. Frank, pp. 177–193, Cambridge Univ. Press, New York.

Milan, S. E., B. Hubert, and A. Grocott (2005), Formation and motion of a transpolar arc in response to dayside and nightside reconnection, *J. Geophys. Res.*, *110*, A01212, doi:10.1029/2004JA010835.

Moen, J., P. Sandholt, M. Lockwood, W. Denig, U. Løvhaug, B. Lybekk, A. Egeland, D. Opsvik, and E. Friis-Christensen (1995), Events of enhanced convection and related dayside auroral activity, *J. Geophys. Res.*, *100*, 23,917–23,934.

Moen, J., N. Gulbrandsen, D. A. Lorentzen, and H. C. Carlson (2007), On the MLT distribution of *F* region polar cap patches at night, *Geophys. Res. Lett.*, *34*, L14113, doi:10.1029/2007GL029632.

Moen, J., Y. Rinne, H. C. Carlson, K. Oksavik, R. Fujii, and H. Opgenoorth (2008), On the relationship between thin Birkeland current arcs and reversed flow channels in the winter cusp/cleft ionosphere, *J. Geophys. Res.*, *113*, A09220, doi:10.1029/2008JA013061.

Provan, G., and T. K. Yeoman (1999), Statistical observations of the MLT, latitude and size of pulsed ionospheric flows with the CUTLASS Finland radar, *Ann. Geophys.*, *17*, 855–867.

Rinne, Y., J. Moen, K. Oksavik, and H. C. Carlson (2007), Reversed flow events in the winter cusp ionosphere observed by the European Incoherent Scatter (EISCAT) Svalbard radar, *J. Geophys. Res.*, *112*, A10313, doi:10.1029/2007JA012366.

Sandholt, P. E., C. J. Farrugia, J. Moen, Ø. Noraberg, B. Lybekk, T. Sten, and T. L. Hansen (1998), A classification of dayside auroral forms and activities as a function of IMF orientation, *J. Geophys. Res.*, *103*, 23,325–23,345, doi:10.1029/98JA02156.

Shiokawa, K., K. Yumoto, K. Hayashi, T. Oguti, and D. J. McEwen (1995), A statistical study of the motions of auroral arcs in the high-latitude morning sector, *J. Geophys. Res.*, *100*, 21,979–21,985, doi:10.1029/95JA01564.

Shiokawa, K., K. Yumoto, N. Nishitani, K. Hayashi, T. Oguti, D. J. McEwen, Y. Kiyama, F. J. Rich, and T. Mukai (1996), Quasi-periodic poleward motions of Sun-aligned auroral arcs in the high-latitude morning sector: A case study, *J. Geophys. Res.*, *101*, 19,789–19,800, doi:10.1029/96JA01202.

Shiokawa, K., T. Ogino, K. Hayashi, and D. J. McEwen (1997), Quasi-periodic poleward motions of morningside Sun-aligned arcs: A multiple-event study, *J. Geophys. Res.*, *102*, 24,325–24,332, doi:10.1029/97JA02383.

Shiokawa, K., Y. Katoh, M. Satoh, M. K. Ejiri, T. Ogawa, T. Nakamura, T. Tsuda, and R. H. Wiens (1999), Development of optical mesosphere thermosphere imagers (OMTI), *Earth Planets Space*, *51*, 887–896.

Shiokawa, K., Y. Katoh, M. Satoh, M. K. Ejiri, and T. Ogawa (2000), Integrating-sphere calibration of all-sky cameras for nightglow measurements, *Adv. Space Res.*, *26*, 1025–1028.

Shiokawa, K., Y. Otsuka, and T. Ogawa (2009), Propagation characteristics of nighttime mesospheric and thermospheric waves observed by optical mesosphere thermosphere imagers at middle and low latitudes, *Earth Planets Space*, *61*, 479–491.

Suzuki, S., K. Shiokawa, K. Hosokawa, K. Nakamura, and W. K. Hocking (2009), Statistical characteristics of polar cap mesospheric gravity waves observed by an all - sky airglow imager at Resolute Bay, Canada, *J. Geophys. Res.*, *114*, A01311, doi:10.1029/2008JA013652.

Valladares, C. E., H. C. Carlson Jr., and K. Fukui (1994), Interplanetary magnetic field dependency of stable Sun-aligned polar cap arcs, *J. Geophys. Res.*, *99*, 6247–6272, doi:10.1029/93JA03255.

Zhu, L., R. W. Schunk, and J. J. Sojka (1997), Polar cap arcs: A review, *J. Atmos. Terr. Phys.*, *59*, 1087–1126.

K. Hosokawa, Department of Communication Engineering and Informatics, University of Electro-Communications, Chofugaoka 1-5-1, Chofu, Tokyo 182-8585, Japan. (hosokawa@ice.uec.ac.jp)

J. I. Moen, Department of Physics, University of Oslo, PO Box 1048, Blindern, N-0316 Oslo, Norway. (j.i.moen@fys.uio.no)

Y. Otsuka and K. Shiokawa, Solar-Terrestrial Environment Laboratory, Nagoya University, Furo-cho, Chikusa-ku, Nagoya 464-8601, Japan. (otsuka@stelab.nagoya-u.ac.jp; shiokawa@stelab.nagoya-u.ac.jp)